

Spin-orbit-coupling-induced backaction cooling in cavity optomechanics with a Bose-Einstein condensate

Kashif Ammar Yasir,^{1,2,*} Lin Zhuang,^{3,†} and Wu-Ming Liu^{1,2,‡}¹*Beijing National Laboratory for Condensed Matter Physics, Institute of Physics, Chinese Academy of Sciences, Beijing 100190, China*²*School of Physical Sciences, University of Chinese Academy of Sciences, Beijing 100190, China*³*School of Physics, Sun Yat-Sen University, Guangzhou 510275, People's Republic of China*

(Received 24 August 2016; published 4 January 2017)

We report a spin-orbit-coupling-induced backaction cooling in an optomechanical system, composed of a spin-orbit-coupled Bose-Einstein condensate trapped in an optical cavity with one movable end mirror, by suppressing heating effects of quantum noises. The collective density excitations of the spin-orbit-coupling-mediated hyperfine states—serving as atomic oscillators equally coupled to the cavity field—trigger strongly driven atomic backaction. We find that the backaction not only revamps low-temperature dynamics of its own but also provides an opportunity to cool the mechanical mirror to its quantum-mechanical ground state. Further, we demonstrate that the strength of spin-orbit coupling also superintends dynamic structure factor and squeezes nonlinear quantum noises, like thermomechanical and photon shot noise, which enhances optomechanical features of the hybrid cavity beyond previous investigations. Our findings are testable in a realistic setup and enhance the functionality of cavity optomechanics with spin-orbit-coupled hyperfine states in the field of quantum optics and quantum computation.

DOI: [10.1103/PhysRevA.95.013810](https://doi.org/10.1103/PhysRevA.95.013810)

I. INTRODUCTION

Cavity optomechanics provides splendid foundations in utilizing mechanical effects of light to couple the optical degree of freedom with the mechanical degree of freedom [1–3]. A pivotal paradigm was to cool vibrational modes of the mechanical degree of freedom to its quantum-mechanical ground state, which has been attempted via laser radiations, electronic feedback, and dynamical backaction [4–12]. The dynamical backaction is the cavity delay induced by the interactions of intracavity radiation pressure and the Brownian motion of the mirror which leads to cool the mirror depending upon detuning [13–16]. The demonstration of cavity optomechanics with other physical objects, like cold atomic gases [17] and Bose-Einstein condensates (BECs) [18–20], opens up various new aspects to further cool vibrational modes through atomic backaction [21–25]. However, thermomechanical heating, due to the quantum noises [26–30], is a major obstacle in achieving an oscillator with long phonon lifetime in the quantum ground state, which we intend to solve by the inclusion of a spin-orbit-(SO-) coupled BEC.

SO coupling, a stunning phenomenon describing interaction between the spin of a quantum particle and its momentum, has made remarkable progress in the last few years [31–33] and is essential to analyze spin-Hall effect [34,35], topological insulators [36–39], and spintronic devices [40]. The demonstration of SO coupling in one-dimensional optical lattices [41–52] and optical cavities [53–55] enables us to utilize this phenomenon in an optomechanical environment. The SO coupling induces significant variations in cavity radiation pressure by separating the atomic mode in hyperfine spin states, which gives rise to self-confinement via dynamical

backaction [1,56–58]. Further, the dynamic structure factor, a phenomenon describing density fluctuations and mean energy of excited quasiparticles, is crucially important in quantum many-body systems [59] and provides an explanation of quasiparticle evolution under noise effects [60–62].

In this paper, we report the SO-coupling-induced backaction cooling mechanism in a hybrid optomechanical cavity with SO-coupled BEC and one moving end mirror in the presence of quantum noises. We show that the SO-coupling-induced features modify intracavity atomic backaction, which not only leads to maneuver low-temperature dynamics of the atomic mode but also helps in ground-state cooling of vibrational modes of the cavity mirror. Further, the coupling of the mechanical mirror with the cavity modifies the eigenenergy spectrum of hyperfine states via transformation of phonons to the atomic degree of freedom and provides a way to tune quantum phase transitions in BECs. Furthermore, we compute the dynamic structure factor by manipulating two frequency autocorrelation of photons leaking out from the cavity and observe the influence of SO coupling on dynamic structure factor.

II. CAVITY OPTOMECHANICS WITH SO-COUPLED BEC

The system consists of a high- Q Fabry-Pérot cavity, with one fixed and one movable mirror, containing an SO-coupled BEC illuminated along the \hat{y} axis and coherently driven by a single-mode optical field with frequency $\omega_p = \omega_R + \delta\omega_R = 8.8 \times 2\pi$ MHz [see Fig. 1(a)]. To produce SO coupling, we chose two internal atomic pseudo-spin-states in $N = 1.8 \times 10^5$ ^{87}Rb bosonic particles having $F = 1$ electronic ground manifold of $5S_{1/2}$ electronic levels labeled as $|\uparrow\rangle = |F = 1, m_F = 0\rangle$ (pseudo-spin-up) and $|\downarrow\rangle = |F = 1, m_F = -1\rangle$ (pseudo-spin-down), as shown in Fig. 1(b). The magnetic 10G bias field B_0 is applied along the cavity axis (\hat{y} axis) to induce Zeeman shift $\hbar\omega_z$, where $\omega_z \approx 4.8 \times 2\pi$ kHz. Two

*kayasir@iphy.ac.cn

†stszhl@mail.sysu.edu.cn

‡wliu@iphy.ac.cn

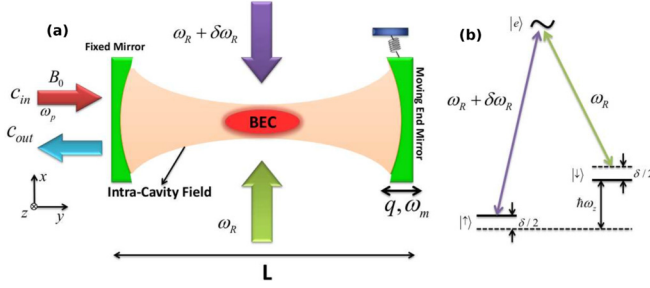


FIG. 1. (a) Schematic diagram of a spin-orbit (SO)-coupled ^{87}Rb Bose-Einstein condensate (BEC) trapped inside a high- Q Fabry-Pérot cavity with one moving end mirror, where the \hat{y} axis is the cavity axis and the \hat{x} axis is the direction of incident Raman beams. (b) Energy-level configuration of SO-coupled BEC.

counterpropagating Raman lasers along the \hat{x} axis, with wavelength $\lambda = 804.1$ nm and detuning $\delta = 1.6E_R$, interact with atomic spin states in opposite direction. The frequencies of these Raman beams are ω_R and $\omega_R + \delta\omega_R$, respectively, with constant frequency difference $\delta\omega_R = \omega_z + \delta/\hbar \simeq 4.8 \times 2\pi$ MHz. $\mathbf{k}_L = \hbar\mathbf{k}_y = \sqrt{2\pi\hbar}/\lambda$ and $E_R = (\hbar k_y)^2/2m_a = 20 \times 2\pi$ kHz represent unitless momentum and energy, respectively. The mechanical mirror is coupled to the cavity mode, oscillating with frequency $\omega_c = 4 \times 2\pi$ MHz and detuning $\Delta_c = \omega_p - \omega_c = \delta\omega_R$, via radiation pressure force [1,18].

The system Hamiltonian consists of three parts, $\hat{H} = \hat{H}_a + \hat{H}_m + \hat{H}_f$. In the strong detuning regime and under the rotating-wave approximation, the many-body Hamiltonian for the atomic mode (H_a) is given as [42,53,54]

$$\hat{H}_a = \int d\mathbf{r} \hat{\psi}^\dagger(\mathbf{r})(H_0 + V_{\text{LAT}})\hat{\psi}(\mathbf{r}) + \frac{1}{2} \int d\mathbf{r} \sum_{\sigma,\sigma'} U_{\sigma,\sigma'} \hat{\psi}_\sigma^\dagger(\mathbf{r})\hat{\psi}_{\sigma'}^\dagger(\mathbf{r})\hat{\psi}_\sigma(\mathbf{r})\hat{\psi}_{\sigma'}(\mathbf{r}), \quad (1)$$

where m_a is the mass of an atom and $\hat{\psi} = [\hat{\psi}_\uparrow, \hat{\psi}_\downarrow]^T$ represents the bosonic field operator for pseudo-spin-up and -down atomic states. $H_0 = \hbar^2\mathbf{k}^2\sigma_0/2m_a + \tilde{\alpha}\mathbf{k}_x\sigma_y + \frac{\delta}{2}\sigma_y + \frac{\Omega_z}{2}\sigma_z$ describes single-particle Hamiltonian containing SO coupling terms [33,63], where $\tilde{\alpha} = E_R/k_L$ is the strength of SO coupling. $\delta = -g\mu_B B_z$ and $\Omega_z = -g\mu_B B_y$ are related to the Zeeman field effects along the \hat{z} and \hat{y} axis, respectively. $\sigma_{x,y,z}$ represents 2×2 Pauli matrices under pseudo-spin rotation and σ_0 is a unit matrix [42,63]. $V_{\text{LAT}} = \hbar\hat{c}^\dagger\hat{c}U_0[\cos^2(kx) + \cos^2(ky)]$ is the intracavity optical lattice under assumption $k_x = k_y = k$ and both atomic states are equally coupled to the cavity because of having same motional quantum state [54,64]. $\hbar\hat{c}^\dagger\hat{c}U_0$ is the optical potential depth with atom-photon coupling $U_0 = g_0^2/\Delta_a$, where g_0 is the vacuum Rabi frequency and Δ_a is far-off detuning between field frequency and atomic transition frequency ω_0 . Here, $\hat{c}(\hat{c}^\dagger)$ are annihilation (creation) operators for the cavity mode. Finally, the last term explains many-body intraspecies and interspecies interactions for atomic spin states, where $\sigma, \sigma' \in \{\uparrow, \downarrow\}$. $U_{\sigma,\sigma'} = 4\pi a_{\sigma,\sigma'}^2 \hbar^2/m_a$ accounts for strength of atom-atom interactions, where $a_{\sigma,\sigma'}$ is the s -wave scattering length.

The Hamiltonian for the moving end mirror is $\hat{H}_m = \hbar\omega_m\hat{b}^\dagger\hat{b} - i\hbar\frac{g_m}{\sqrt{2}}\hat{c}^\dagger\hat{c}(\hat{b}^\dagger + \hat{b})$, where the first term describes the motion of the mechanical mirror with frequency ω_m and $\hat{b}(\hat{b}^\dagger)$ are annihilation (creation) operators for the mechanical mirror with commutation relation $[\hat{b}^\dagger, \hat{b}] = 1$. The second term accommodates mechanical mirror coupling with cavity mode with coupling strength $g_m = \sqrt{2}(\omega_c/L)x_0$, where $x_0 = \sqrt{\hbar/2m\omega_m}$ is the zero-point motion of the mechanical mirror having mass m . $\hat{H}_c = \hbar\Delta_c\hat{c}^\dagger\hat{c} - i\hbar\eta(\hat{c} - \hat{c}^\dagger)$, where the first term is the strength of the cavity mode and the second part is associated with its coupling with external pump field with strength $|\eta| = \sqrt{P\kappa/\hbar\omega_p}$, where P is the input field power.

We substitute plane-wave ansatz $\hat{\psi}(\mathbf{r}) = e^{i\mathbf{k}\cdot\mathbf{r}}\hat{\phi}$, where $\hat{\phi} = [\hat{\phi}_\uparrow, \hat{\phi}_\downarrow]^T$, in atomic mode Hamiltonian H_a by considering homogeneous atomic modes distribution with normalization condition $|\hat{\phi}_\uparrow|^2 + |\hat{\phi}_\downarrow|^2 = N$. We assume that the strengths of intraspecies interactions of both spin states are equal with each other and are defined as $U_{\uparrow,\uparrow} = U_{\downarrow,\downarrow} = U$. Similarly, interspecies interactions can be modeled as $U_{\uparrow,\downarrow} = U_{\downarrow,\uparrow} = \varepsilon U$, where parameter ε depends upon the incident laser configuration [33]. Under these considerations, we solve equation H_a and compute quantum Langevin equations for the system by using standard quantum noise operators to include quantum noises and dissipations associated with the system [21,50]. The quantum Langevin equation helps us in developing the coupled and time-dependent set of equations, containing noise operators for optical, mechanical, and atomic degrees of freedom:

$$\frac{d\hat{c}}{dt} = \hat{c} = \left(i\tilde{\Delta} + i\frac{g_m}{\sqrt{2}}(\hat{b} + \hat{b}^\dagger) - ig_a\hat{\phi}^\dagger\hat{\phi} - \kappa \right) \hat{c} + \eta + \sqrt{2\kappa}a_{\text{in}}, \quad (2)$$

$$\frac{d\hat{b}}{dt} = \hat{b} = -\omega_m\hat{b} - \frac{g_m}{\sqrt{2}}\hat{c}^\dagger\hat{c} - \gamma_m\hat{b} + \sqrt{\gamma_m}f_m, \quad (3)$$

$$\frac{d\hat{\phi}}{dt} = \hat{\phi} = \left(\frac{\hbar\mathbf{k}^2\sigma_0}{2m} + \tilde{\alpha}\mathbf{k}_x\sigma_y + \frac{\delta}{2}\sigma_y + \frac{\Omega_z}{2}\sigma_z - \gamma_a + g_a\hat{c}^\dagger\hat{c} \right) \hat{\phi} + \frac{1}{2}U\hat{\phi}^\dagger\hat{\phi}\hat{\phi} + \frac{1}{2}\varepsilon U\hat{\phi}_\uparrow^\dagger\hat{\phi}_\sigma\hat{\phi}_\sigma + \sqrt{\gamma_a}f_a, \quad (4)$$

where $\tilde{\Delta} = \Delta_c - NU_0/2$ is the modified detuning of the system and \hat{c}_{in} is the Markovian input noise operator associated with intracavity field, having zero average $\langle \hat{c}_{\text{in}}(t) \rangle = 0$ and delta correlation $\langle \hat{c}_{\text{in}}(t)\hat{c}_{\text{in}}^\dagger(t') \rangle = \delta(t-t')$ under the condition $\hbar\omega_c \gg k_B T$. The term γ_m describes the mechanical energy decay rate of the moving end mirror and f_m is the noise operator (or zero-mean Langevin-force operator) connected with the Brownian motion of the mechanical mirror and can be defined by using non-Markovian correlation [21,50] $\langle f_m(t)f_m(t') \rangle = \frac{\gamma_m}{2\pi\omega_m} \int d\omega e^{-i\omega(t-t')} [1 + \coth(\frac{\hbar\omega}{2k_B T})]$. The external harmonic trapping potential of the condensate, which we have ignored so far because it appeared to be spin independent, causes the damping of the atomic motion. The parameter γ_a represents such damping of atomic dressed states motion while f_a is the associated noise operators assumed to be Markovian with delta correlation $\langle f_a(t)f_a^\dagger(t') \rangle = \delta(t-t')$ under the condition $\hbar\Omega \gg k_B T$. Further, $\sigma, \sigma' \in \{\uparrow, \downarrow\}$, and $g_a = \frac{\omega_c}{L}\sqrt{\hbar/m_{\text{bec}}4\omega_r}$ is the coupling of atomic mode with

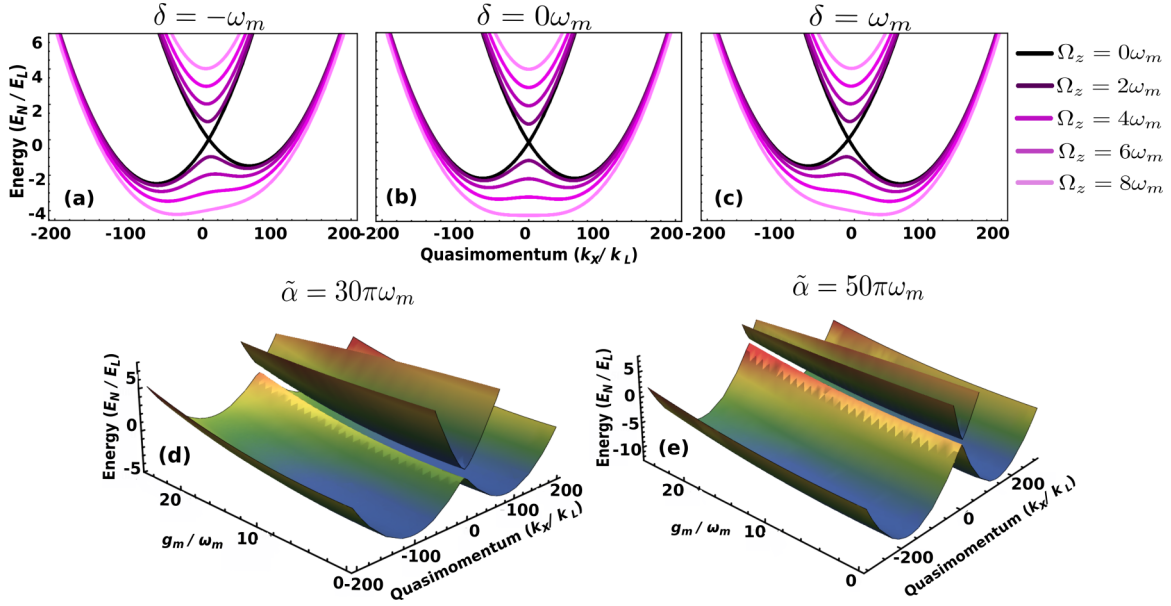


FIG. 2. (a–c) Eigenenergies spectrum E_N of a spin-orbit (SO)-coupled Bose-Einstein condensate (BEC) as a function of quasimomentum $\mathbf{k}_x/\mathbf{k}_L$ for different Ω_z/ω_m and δ/ω_m , when $g_m/\omega_m = 0.1$ and $\alpha/\omega_m = 20\pi$. (It should be noted that we consider $\mathbf{k}_y = \mathbf{k}_z = 0$ because SO coupling is occurring only in the direction of the \hat{x} axis.) The black curve represents dispersion at $\Omega_z/\omega_m = 0$ while magenta shaded curves (from darkest to lightest) correspond to $\Omega_z/\omega_m = 2, 4, 6, 8$, respectively. (a,b,c) Behavior of dispersion E_N for $\delta/\omega_m = -1, 0, 1$, respectively. (d,e) Dispersion E_N vs $\mathbf{k}_x/\mathbf{k}_L$ and g_m/ω_m , with $\alpha/\omega_m = 30\pi$ and $\alpha/\omega_m = 50\pi$, respectively, at $\Omega_z = \omega_m$ and $\delta/\omega_m = 0$. The other parameters used are $U/\omega_m = 5.5$, $\varepsilon/\omega_m = 0.1$, $\kappa/\omega_m = 0.1$, $\gamma_a/\omega_m = 0.01$, $\gamma_m/\omega_m = 0.05$, and mechanical mirror frequency $\omega_m \approx \omega_c - \omega_p$.

intracavity field, having effective BEC frequency $\Omega = 4\omega_r$ and mass $m_{\text{bec}} = \hbar\omega_c^2/(L^2U_0^2\omega_r)$, where $\omega_r = 3.8 \times 2\pi$ kHz is the recoil frequency of atoms and $L = 1.25 \times 10^{-4}$ m is the cavity length.

III. CONDENSATE DISPERSION SPECTRUM

The eigenenergy spectrum is calculated from time-dependent quantum Langevin equations (for details see Appendix A). The SO coupling will create two minima corresponding to lowest-energy levels of atomic spin states, as illustrated in Fig. 2. At $\Omega_z/\omega_m = 0$, no band gap appears between lower and upper dispersion states causing the phase mixing of atomic dressed states. However, in presence of Raman coupling, the band gap between upper $E_N > 0$ and lower $E_N < 0$ dispersion states appears in the form of a Dirac cone which increases with the increase in Raman coupling. The higher values of Ω_z/ω_m merge two minima corresponding to the dressed states into single minima causing quantum phase transitions from the mixed phase to a separate phase of the atomic mode. It can also be seen that the nonzero Raman detuning $\delta/\omega_m \neq 0$ leads to the symmetry breaking of dispersion over quasimomentum. For the small value of Raman coupling ($\Omega_z < 4\omega_m$), the dispersion appears in the form of a double-well potential in the quasimomentum which leads to the zero group velocity of atoms [65]. The asymmetric behavior indicates rapid population transfer and enhancement in band-gap-induced features of hyperfine states in the cavity environment. Moreover, it is noted that because of cavity confinement, the atomic quasimomentum $\mathbf{k}_x/\mathbf{k}_L$ interacts with the optical mode along cavity axes. Thus, SO-coupled BECs

face an anisotropic potential which leads towards spatial spread of the BEC energy spectrum along the cavity axis, as can be seen in Fig. 2.

The coupling between atomic states and intracavity potential is disturbed by the existence of the mechanical mirror, and vice versa, when the atomic modes become resonant with the optical sideband. At this point, atomic spin states will absorb some phonons emitted by the mechanical mirror via the cavity mode and will behave as a phononic well. Therefore, the increase in mirror-field coupling gives rise to atomic-state energy levels, as shown in Figs. 2(d) and 2(e), which provides precise control over the dispersion relation of the atomic energy spectrum and quantum phase transitions of the BEC.

IV. ATOMIC DENSITY-NOISE SPECTRUM

We calculate the density-noise spectrum (DNS) of atomic spin states by taking the two frequency autocorrelation of the frequency domain solution of quantum Langevin equations, $S_{\uparrow,\downarrow}(\omega, \Delta) = \frac{1}{4\pi} \int e^{-i(\omega+\omega')t} \langle \delta\hat{q}_{\uparrow,\downarrow}(\omega)\delta\hat{q}_{\uparrow,\downarrow}(\omega') + \delta\hat{q}_{\uparrow,\downarrow}(\omega')\delta\hat{q}_{\uparrow,\downarrow}(\omega) \rangle d\omega'$, where $\delta\hat{q}_{\uparrow,\downarrow}$ are dimensionless position quadratures of spin states defined as $\delta\hat{q}_{\uparrow,\downarrow} = \frac{1}{\sqrt{2}}(\hat{\phi}_{\uparrow,\downarrow} + \hat{\phi}_{\uparrow,\downarrow}^\dagger)$. Here the effective system detuning is $\Delta = \tilde{\Delta} - g_m q_s + g_a N$, where q_s is the steady-state position quadrature of the mechanical mirror, while $G_m = \sqrt{2}g_m|c_s|$ and $G_a = \sqrt{2}g_a|c_s|$ are the effective couplings of the intracavity field with the mechanical mirror and atomic modes, respectively, tuned by the steady-state cavity mode amplitude $c_s = \frac{\eta}{\kappa+i\Delta}$ (for detailed calculations see Appendices B and C). By considering the correlation operators of Markovian and Brownian noises in

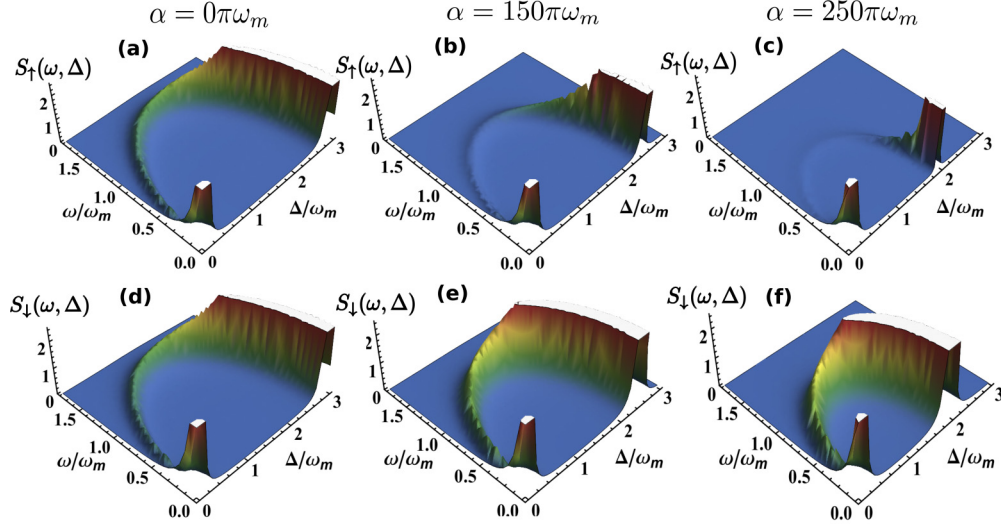


FIG. 3. (a–c) DNS $S_{\uparrow}(\omega, \Delta)$ as a function of Δ/ω_m and ω/ω_m for $\alpha/\omega_m = 0\pi, 150\pi$, and 250π , respectively, when $\Omega_z = \omega_m$, $\delta/\omega_m = 1$, and $G_a/\omega_m = 28.5$. (Note: The color configuration corresponds to the strength of DNS.) Similarly, (d–f) demonstrate DNS $S_{\downarrow}(\omega, \Delta)$ for $\alpha/\omega_m = 0\pi, 150\pi$, and 250π , respectively. Here $G_m/\omega_m = 1.5$, $\Omega/\omega_m = 70.8$, $\omega_m = 3.8 \times 2\pi$ kHz and the thermal reservoir temperature is taken as $T = 300$ K.

the frequency domain [21,22,66,67], we plot the DNS for pseudo-spin-up and spin-down atomic states as shown in Fig. 3.

The inclusion of SO coupling in trapped atoms modifies atomic backaction generated by the interaction of intracavity radiation pressure with the BEC. These modifications enhance the cavity induced self-regulatory mechanism of the atomic mode. In the absence of SO coupling ($\alpha/\omega_m = 0\pi$), both $S_{\uparrow}(\omega, \Delta)$ and $S_{\downarrow}(\omega, \Delta)$ behave in a similar way as shown in Figs. 3(a) and 3(d) [21,22], where $\alpha = \tilde{\alpha}k_x$ is the effective strength of SO coupling. Both the cooling as well as heating mechanisms are observable because the area under $S_{\uparrow}(\omega, \Delta)$ describes the effective temperature of the atomic mode, as shown in effective temperature calculation of the mechanical mirror in the next section. One can observe a semicircular structure appearing with the increase in Δ/ω_m caused by the redshift in the peak frequency of $S_{\uparrow}(\omega, \Delta)$. The height of the structure initially decreases with increase in Δ/ω_m but shortly again starts rising along the semicircular structure. The optimal cooling is achieved at $\Delta = \omega_m/2$ with a considerable shrink in the area underneath the atomic DNS.

In the presence of α/ω_m , $S_{\uparrow}(\omega, \Delta)$ and $S_{\downarrow}(\omega, \Delta)$ start behaving in a different manner because of the emergence of the Zeeman shift among the hyperfine atomic states with SO coupling. For $S_{\uparrow}(\omega, \Delta)$, the height of the semicircular structure is suppressed due to the energy transformation via intracavity potential, as can be seen in Figs. 3(b) and 3(c), where $\alpha/\omega_m = 150\pi$ and 250π , respectively. The optimal cooling point is now shifted to $\Delta/\omega_m = 1$. The existence of SO coupling not only decreases the area underneath $S_{\uparrow}(\omega, \Delta)$ but also suppresses the radius of that semicircular structure providing controlled cooling of the atomic mode. However, at $\alpha/\omega_m \neq 0\pi$, $S_{\downarrow}(\omega, \Delta)$ behave differently because of more interaction with quantum noise effects, as shown in Figs. 3(e) and 3(f). Now the height of the semicircular structure appearing in $S_{\downarrow}(\omega, \Delta)$ is being increased with increase in SO coupling. The

SO-coupling-induced Zeeman field effect generates the energy gap between dressed states by increasing and decreasing the ground-state energies of pseudo-spin-down and pseudo-spin-up states, respectively. Therefore, by increasing SO coupling, the spin-down state will interact with more noise effects and get heated because of having more ground-state energy as compared to the spin-up state. However, it can be controlled by varying system parameters and the radius of the semicircular structure still appears to be decreasing with SO coupling due to cavity mediated self-confinement via backaction. Further, in the presence of SO coupling, atom-atom interactions will affect similarly the low-temperature dynamics of the atomic mode, as explained in Appendix E.

V. MECHANICAL MIRROR COOLING

The effective temperature of the mechanical mode (T_{eff}) is calculated by the formula $T_{\text{eff}} = \langle E_m \rangle / k_B$, where $\langle E_m \rangle = m\omega_m^2 \langle \delta\hat{q}^2 \rangle / 2 + \langle \delta\hat{p}^2 \rangle / 2m = m\omega_m^2 (n_{\text{eff}} + 1/2)$ corresponds to the mean energy which is experimentally measured by calculating the area underneath the DNS of the mechanical mirror $S_m(\omega, \Delta) = \frac{1}{4\pi} \int e^{-i(\omega+\omega')t} \langle \delta\hat{q}(\omega) \delta\hat{q}(\omega') + \delta\hat{q}(\omega') \delta\hat{q}(\omega) \rangle d\omega'$, where $\delta\hat{q}$ is the dimensionless position quadrature of the mechanical mirror defined as $\delta\hat{q} = \frac{1}{\sqrt{2}}(\hat{b} + \hat{b}^\dagger)$ (for detail see Appendices B and C). n_{eff} is the effective phonon number which should be less than 1 in order to achieve ground-state cooling. The position and momentum variances are related to the DNS, $\langle \delta\hat{\mathcal{R}}^2 \rangle = \frac{1}{2\pi} \int S_{\mathcal{R}}(\omega, \Delta) d\omega$, where \mathcal{R} is a generic operator representing the position $\delta\hat{q}$ and momentum $\delta\hat{p}$ quadrature of the mechanical mirror. Here the DNS of the mechanical mirror in momentum space is defined as $S_{m(p)}(\omega, \Delta) = m^2 \omega_m^2 S_m(\omega, \Delta)$, where m is the effective mass of the mechanical mirror.

The cooling mechanism for the mechanical mirror, which can simply be explained by thermodynamic arguments, only occurs when the intracavity optical sideband is centered at

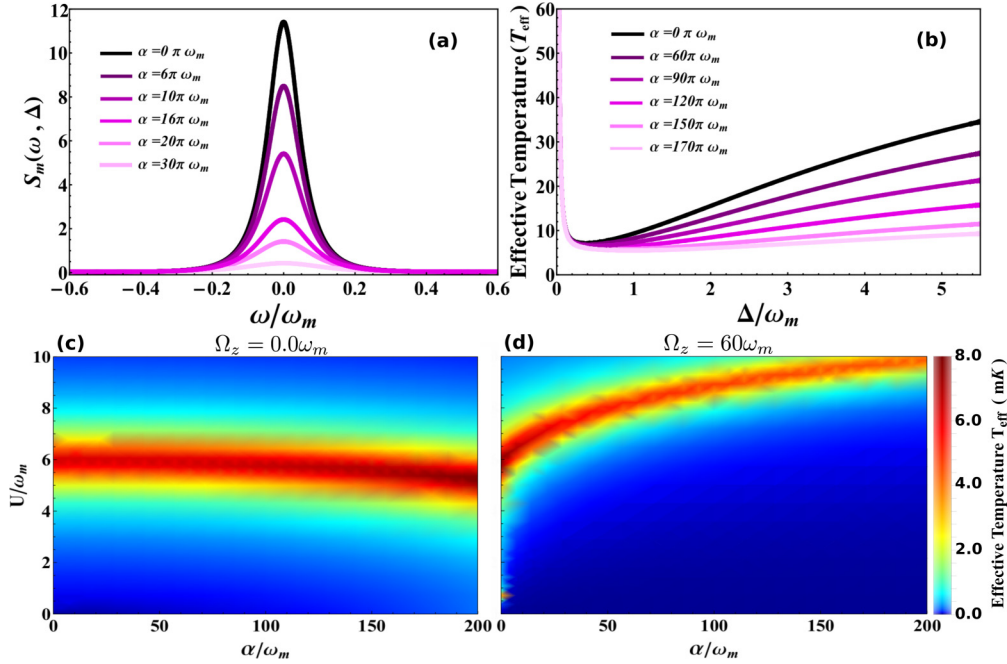


FIG. 4. (a) $S_m(\omega, \Delta)$ vs normalized frequency ω/ω_m at $\Delta/\omega_m = 1.8$, $G_m/\omega_m = 10$, and $G_a/\omega_m = 20$. The black curve is for $\alpha/\omega_m = 0\pi$ and magenta curves from dark shade to light shade represent $\alpha/\omega_m = 6\pi, 10\pi, 16\pi, 20\pi$, and 30π , respectively. (b) T_{eff} (in units of mK) vs Δ/ω_m at $\omega/\omega_m = 0.1$, $G_m/\omega_m = 10$, and $G_a/\omega_m = 5$. Similarly, the black corresponds to $\alpha/\omega_m = 0\pi$ while shaded curves from darkest to lightest represent $\alpha/\omega_m = 60\pi, 90\pi, 120\pi, 150\pi$, and 170π , respectively. (c,d) T_{eff} , as a function of α/ω_m and U/ω_m , at $\Omega_z/\omega_m = 0$ and 80 , respectively. Here, $G_m/\omega_m = 18$, $G_a/\omega_m = 16$, and $\alpha/\omega_m = 30\pi$.

ω_m , which is in fact a resolved-sideband regime. Therefore, the BEC should also oscillate at optical sideband frequency in order to absorb excitation energies of the mirror from the cavity mode, otherwise mirror temperature will be unaffected. The implication of SO coupling splits the atomic mode into dressed spin states—acting like two atomic mirrors equally coupled to the cavity—which will modify atomic backaction inside the cavity. This phenomenon enables us to transfer more excitation energies in the form of phonons from the mechanical mirror to the atomic degree of freedom. Figure 4(a) illustrates such effects where the suppression of the mechanical mirror DNS $S_m(\omega, \Delta)$ can be seen with the increase in SO coupling. The SO coupling suppresses the heating effects induced by the Brownian motion of the mirror and enhances backaction cooling of the oscillating mirror. Figure 4(a) demonstrates the mirror DNS at system detuning $\Delta/\omega_m = 1.8$. If we change system detuning, it will modify the mirror DNS by increasing or decreasing its strength but the effects of SO coupling on the mirror DNS will remain the same, as discussed in Appendix F. Further, the SO coupling reduces T_{eff} over a wide range of detuning because of energy transformation via modified backaction, as shown in Fig. 4(b), where optimal temperature is decreasing with the increase in SO coupling. This implies, like atomic-field coupling and atom-atom interactions (as discussed in Appendix G) [13–16,23–25], SO coupling significantly alters ground-state properties of the mechanical mirror. Thus, SO coupling provides another handle to achieve and sustain ground-state cooling which is even beyond the previous backaction cooling mechanism.

To further analyze the influence of SO-coupled dressed states on the mechanical mirror, we plot T_{eff} , as a function of

U/ω_m and α/ω_m , in the absence [Fig. 4(c)] and in the presence [Fig. 4(d)] of Raman coupling Ω_z/ω_m . At $\Omega_z/\omega_m = 0$, the maximum value of T_{eff} appears to be approximately centered at $U/\omega_m \approx 6$ and remains saturated with increase in α/ω_m . One can state that the maximum value of T_{eff} shows a kind of localized behavior with SO coupling which is similar to the results presented in Ref. [23]. On the other hand, in the presence of Raman coupling, T_{eff} shows squeezed and exponential behavior with α/ω_m , as illustrated in Fig. 4(d). The SO coupling in the presence of strong Raman coupling, which transforms the atomic dispersion spectrum into single minima, absorbs more mirror excitation energies and manipulates atom-atom interactions effects on mirror temperature by modifying backaction. Intuitively speaking, the higher values of Raman coupling change the quantum phase of trapped atoms, causing the alteration in their many-body interactions as well as in SO coupling effects. Therefore, the suppressed and nonlinear behavior of T_{eff} is caused by the emergence of band-gap-induced quantum phase transitions of the BEC and can be further enhanced by increasing Ω_z/ω_m , providing control over temperature of the mechanical mirror [13,14,23].

VI. DYNAMIC STRUCTURE FACTOR

We analyze the dynamic structure factor by computing Fourier domain autocorrelations of light leaking out of the cavity. The resultant dynamic structure factor is given as [62] $S_D(k, \omega) = \frac{4(\kappa^2 + \Delta^2)}{N\eta^2} [\frac{1}{2\pi} S_{\text{out}}(P, \omega) + n_s^2 \delta(\omega)]$, where n_s is the steady-state photon number and $S_{\text{out}}(P, \omega)$ is the DNS of the outgoing optical mode (see Appendix D). The frequency ω is referred to the shifted frequency of the input field after

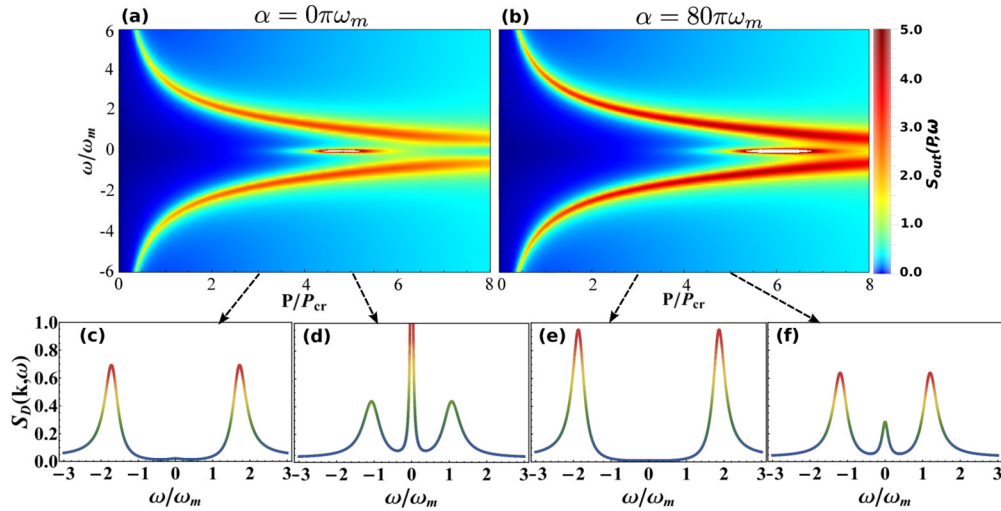


FIG. 5. (a,b) DNS of optical field leaking out of cavity $S_{\text{out}}(P, \omega)$ (in units of W/Hz), vs P/P_{cr} and ω/ω_m , for $\alpha/\omega_m = 0\pi$ and 80π , respectively. (c–f) Dynamic structure factor (in units of 1/Hz) corresponding to the out-going optical mode DNS vs ω/ω_m for different values of P/P_{cr} . SO coupling $\alpha/\omega_m = 0\pi$ (80π) for (c,d), while the strength of SO coupling is $\alpha/\omega_m = 80\pi$ for (e,f). Here $G_m/\omega_m = 1.5$, $G_a/\omega_m = 0.9$, $U/\omega_m = 5.5$, and $\delta/\omega_m = 0$.

interacting with the system which causes inelastic photon scattering.

In the absence of SO coupling, $S_{\text{out}}(P, \omega)$ contains two sidebands at $\omega < 0\omega_m$ and $\omega > 0\omega_m$ caused by the incoherent creation and annihilation of quasiparticles [62], respectively [see Fig. 5(a)]. If we increase the input power, both the sidebands tend to move towards $\omega = 0\omega_m$ because of quantum fluctuations which decrease the spectral densities of quasiparticles. Intuitively, it is referred to the scattering of the intracavity optical mode at Bragg planes in the density-modulated cloud [60,68]. Both the sidebands seem to get mixed with each other due to the presence of another secondary structure approximately at $P \approx 6P_{\text{cr}}$. The secondary structure, which is centered at $\omega = 0\omega_m$, is caused by associated quantum noises [62]. In the presence of SO coupling, the secondary structure is shifted to $P \approx 7P_{\text{cr}}$ due to the modifications in the inelastic scattering of the cavity mode by atomic spin-phase transitions [59], as shown in Fig. 5(b). The spectral densities of both sidebands as well as secondary structure are also increased due to the addition of quasiparticles excited by the SO coupling.

The dynamic structure factor $S_D(k, \omega)$ at power ratio $P/P_{\text{cr}} = 3$ shows two sidebands at $\omega \approx -2\omega_m$ and $\omega \approx 2\omega_m$ corresponding to creation and annihilation of quasiparticles, respectively, as shown in Fig. 5(c). Another, comparatively small, fluctuating structure can be seen at $\omega = 0\omega_m$ induced by the quantum noise effects, which verifies the experimental finding of the dynamic structure factor in Ref. [62]. If we increase the input field power, the dynamic structure factor will be suppressed by the increase in system fluctuations and the sidebands will move towards $\omega = 0\omega_m$, as shown in Fig. 5(d). However, the strength of the structure appearing at $\omega = 0\omega_m$ is increased because of quantum noise effects. Interestingly, these effects can be suppressed by SO coupling because of enhanced intracavity atomic backaction [see Figs. 5(e) and 5(f)], which leads to the enhancement of the sideband spectrum.

In order to further understand the influence of SO coupling as well as cavity mediated long-range atom-atom interactions,

we plot $S_D(k, \omega)$ for multiple values of SO coupling and atom-atom interactions. Figures 6(a) and 6(b) carry $S_D(k, \omega)$ as a function of normalized frequency for different strengths of α/ω_m and U/ω_m , respectively, at input field power $P/P_{\text{cr}} = 5$. It can be clearly seen that by increasing the SO coupling and atom-atom interactions, the sidebands are enhanced and shifted away from $\omega = 0\omega_m$ due to the addition of quasiparticles. However, quantum noise fluctuations, appearing at $\omega \approx 0$, are now being suppressed by increasing α/ω_m and U/ω_m causing enhancement in optomechanical applications. Here, it should be noted that the strength of atom-atom interactions defines interspecies as well as intraspecies interactions and the frequency of the atomic mode is directly proportional to the strength of interactions \sqrt{U} [23]. Therefore, like SO coupling, atom-atom interactions have significant influence on the intracavity atomic backaction which leads to the enhancement in inelastic scattering of the cavity mode. Thus, the inclusion of SO coupling purifies the dynamic structure factor by squeezing quantum noises.

VII. CONCLUSION

We demonstrate SO-coupling-induced backaction cooling in cavity optomechanics with SO-coupled BECs. The SO coupling modifies dynamical backaction which enhances the low-temperature profile of the atomic mode by squeezing associated noises. It has been shown that the existence of SO coupling leads to a cool vibrating end mirror to its quantum-mechanical ground state. Further, by computing the dynamic structure factor, we have shown that the SO coupling enables us to manage and implement noiseless quasiparticles. Likewise, the mechanical mirror gives rise to the eigenenergy spectrum of atomic states providing control over quantum phase transitions. We chose a particular set of parameters and procedures very close to the present experimental ventures, which makes our study experimentally feasible. Our findings constitute a significant step towards the utilization of

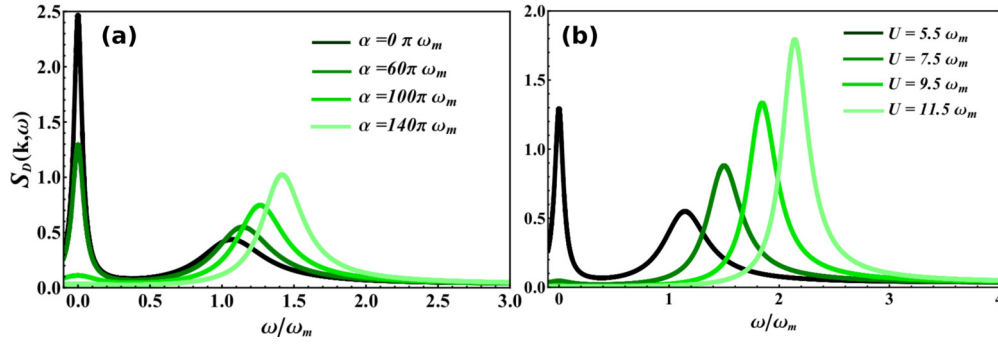


FIG. 6. The dynamic structure factor $S_D(k, \omega)$ (in units of 1/Hz) as a function of ω/ω_m for different strengths of α/ω_m at $U = 5.5\omega_m$ (a) and atom-atom interactions U/ω_m at $\alpha = 10\pi\omega_m$ (b). The input field power ratio is fixed to $P/P_{cr} = 4$ and the remaining coupling strengths are the same as in Fig. 5. In (a), the green shaded curves from darkest to lightest correspond to the SO coupling $\alpha/\omega_m = 0\pi, 60\pi, 100\pi$, and 140π , respectively. Similarly, in (b), green curves (from dark shade to light shade) carry the influence of atom-atom interactions with strengths $U/\omega_m = 5.5, 7.5, 9.5$, and 11.5 , respectively.

SO-coupled BEC optomechanics in the field of quantum optics and quantum information.

ACKNOWLEDGMENTS

This work was supported by the NKRDP under Grant No. 2016YFA0301500; National Natural Science Foundation of China under Grants No. 11434015, No. 61227902, No. 61378017, and No. KZ201610005011; SKLQOQOD under Grant No. KF201403; and SPRPCAS under Grants No. XDB01020300 and No. XDB21030300. We also acknowledge financial support from the CAS-TWAS president's fellowship program.

APPENDIX A: ATOMIC EIGENERGIES CALCULATION

Here we provide some details about energy dispersion calculation of atomic states. By adopting a mean-field approximation, we consider the intracavity field in steady state and replace the intracavity field operator by its expectation value $\hat{c} \rightarrow \langle c \rangle \equiv c_s$. To calculate energy dispersion E_N of atomic modes, we define E_N as the solution of nonlinear quantum Langevin equations for the BEC and replace the time derivative id/dt with eigenenergy E_N . After performing some mathematics and applying Pauli matrices, the coupled Langevin equations will take the form [33,50,55]

$$n_s = c_s^\dagger c_s = \frac{\eta}{\kappa^2 + \left[\tilde{\Delta} - \frac{g_m}{\sqrt{2}}(\hat{b}^\dagger + \hat{b}) + g_a(\hat{\phi}_\uparrow^\dagger \hat{\phi}_\uparrow + \hat{\phi}_\downarrow^\dagger \hat{\phi}_\downarrow) \right]^2}, \quad (\text{A1})$$

$$\hat{b}_s = \frac{g_m c_s^\dagger c_s}{\sqrt{2}(i\omega_m + \gamma_m)}, \quad \hat{b}_s^\dagger = \frac{g_m c_s^\dagger c_s}{\sqrt{2}(-i\omega_m + \gamma_m)}, \quad (\text{A2})$$

$$E_N \begin{pmatrix} \hat{\phi}_\uparrow \\ \hat{\phi}_\downarrow \end{pmatrix} = \begin{pmatrix} \frac{\hbar \mathbf{k}^2}{2m} + \frac{\Omega_z}{2} + g_a c_s^\dagger c_s + \frac{1}{2} U N - \gamma_a & -i(\alpha \mathbf{k}_x + \frac{\delta}{2}) + \frac{1}{2} U(\epsilon - 1) \hat{\phi}_\downarrow^\dagger \hat{\phi}_\uparrow \\ i(\alpha \mathbf{k}_x + \frac{\delta}{2}) + \frac{1}{2} U(\epsilon - 1) \hat{\phi}_\uparrow^\dagger \hat{\phi}_\downarrow & \frac{\hbar \mathbf{k}^2}{2m} - \frac{\Omega_z}{2} + g_a c_s^\dagger c_s + \frac{1}{2} U N - \gamma_a \end{pmatrix} \begin{pmatrix} \hat{\phi}_\uparrow \\ \hat{\phi}_\downarrow \end{pmatrix}, \quad (\text{A3})$$

where n_s is the steady-state photon number inside the cavity and \hat{b}_s is the steady-state quadrature for mechanical mirror. For simplicity, we have ignored quantum noises associated with the system while calculating eigenenergies of the atomic mode. Under number conservation condition $|\hat{\phi}_\uparrow|^2 + |\hat{\phi}_\downarrow|^2 = 1$, we substitute steady-state mechanical mirror operators into Eq. (A1) and simplify in terms of n_s as

$$L_2 n_s^3 + 2L_1 L_2 n_s^2 + K n_s = \eta^2 \quad (\text{A4})$$

where

$$L_1 = \Delta_c + g_a, \quad (\text{A5})$$

$$L_2 = \frac{\gamma_m g_m^2}{\omega_m^2 + \gamma_m^2}, \quad (\text{A6})$$

$$K = \kappa^2 + L_1^2. \quad (\text{A7})$$

Now, by assuming eigenenergies of the moving end mirror and atomic mode independent by keeping the mechanical mirror in steady state, we rewrite Eq. (A3), for $\hat{\phi}_\uparrow$ and $\hat{\phi}_\downarrow$, as

$$E_N \begin{pmatrix} \hat{\phi}_\uparrow \\ \hat{\phi}_\downarrow \end{pmatrix} = \begin{pmatrix} h_1 & w + \frac{1}{2} U(\epsilon - 1) \hat{\phi}_\downarrow^\dagger \hat{\phi}_\uparrow \\ w^* + \frac{1}{2} U(\epsilon - 1) \hat{\phi}_\uparrow^\dagger \hat{\phi}_\downarrow & h_2 \end{pmatrix} \begin{pmatrix} \hat{\phi}_\uparrow \\ \hat{\phi}_\downarrow \end{pmatrix}, \quad (\text{A8})$$

where

$$h_{1,2} = \frac{\hbar \mathbf{k}_x^2}{2m} \pm \frac{\Omega_z}{2} + g_a n_s + \frac{1}{2} U N - \gamma_a, \quad (\text{A9})$$

$$w = \alpha \mathbf{k}_x + \frac{\delta}{2}. \quad (\text{A10})$$

By dividing the first line of Eq. (A8) with the conjugate of the second line, we obtain

$$\frac{E_N - h_1}{E_N - h_2} |\hat{\phi}_\uparrow|^2 = |\hat{\phi}_\downarrow|^2. \quad (\text{A11})$$

Further, by denoting $s = \frac{E_N - h_1}{E_N - h_2}$ and using the number conservation condition, we calculate $|\hat{\phi}_\uparrow|^2$ and $|\hat{\phi}_\downarrow|^2$ as

$$|\hat{\phi}_\uparrow|^2 = \frac{1}{s+1}, \quad (\text{A12})$$

$$|\hat{\phi}_\downarrow|^2 = \frac{s}{s+1}, \quad (\text{A13})$$

and by substituting these values in the first line of Eq. (A8) we obtain

$$(E_N - h_1)^2 - \frac{U(\epsilon - 1)(E_N - h_2)s}{s+1} + \frac{U^2(\epsilon - 1)^2 s^2}{4(s+1)^2} = s w^2. \quad (\text{A14})$$

Finally, by numerically finding roots of steady-state photon number n_s from Eq. (A4) and substituting them into Eq. (A14), we plot the roots of eigenenergies versus quasimomentum \mathbf{k}_x , as shown in Fig. 2. (Note that we consider $\mathbf{k}_y = \mathbf{k}_z = 0$ because SO coupling is occurring only in the direction of \hat{x} -axis.)

APPENDIX B: LANGEVIN EQUATIONS AND FREQUENCY DOMAIN SOLUTIONS

The coupled Langevin equations of the system contain nonlinear terms in the form of coupling among different degrees of freedom and noises associated with the system. By considering an intense external pump field, these equations can be linearized with the help of quantum fluctuations as $\hat{\mathcal{O}}(t) = \mathcal{O}_s + \delta\mathcal{O}(t)$, where \mathcal{O} can be any operator of the system, \mathcal{O}_s represents steady-state value, and $\delta\mathcal{O}(t)$ is the first-order quantum fluctuation. During these calculations for simplicity, we assume that both the atomic states, spin-up and spin-down, have equal amount of particles, i.e., $\hat{\phi}_\uparrow^\dagger \hat{\phi}_\uparrow = \hat{\phi}_\downarrow^\dagger \hat{\phi}_\downarrow = N/2$. Furthermore, we define system quadratures in the form of dimensionless position and momentum quadratures as $\hat{q}_O = \frac{1}{\sqrt{2}}(\hat{O} + \hat{O}^\dagger)$ and $\hat{p}_O = \frac{i}{\sqrt{2}}(\hat{O} - \hat{O}^\dagger)$, respectively (O is a generic operator) having commutation relation $[\hat{q}_O, \hat{p}_O] = i$ which reveals the value of scaled Planck's constant $\hbar = 1$. Now the linearized Langevin equations are defined in the form of $\dot{\mathcal{X}} = \mathcal{K}\mathcal{X} + \mathcal{F}$, where vector $\mathcal{X} = [\delta q_c(t), \delta p_c(t), \delta q(t), \delta p(t), \delta q_\uparrow(t), \delta p_\uparrow(t), \delta q_\downarrow(t), \delta p_\downarrow(t)]^\top$ contains position and momentum quadratures of the system (here p and q with \uparrow and \downarrow indicate atomic states, with c indicating the cavity mode and without anything indicating the mechanical mirror's momentum and position quadrature) and vector $\mathcal{F} = [\sqrt{2\kappa} q_c^{\text{in}}, \sqrt{2\kappa} p_c^{\text{in}}, 0, 2\sqrt{\gamma_m} f_m, 0, 2\sqrt{\gamma_a} f_a, 0, 2\sqrt{\gamma_a} f_a]^\top$ defines noises associated with the system. In following, we have omitted cap from position and momentum quadratures for simplicity. The matrix \mathcal{K} contains dynamical parameters associated with the system

$$\mathcal{K} = \begin{pmatrix} -\kappa & \Delta & 0 & 0 & 0 & 0 & 0 & 0 & 0 \\ \Delta & -\kappa & -G_m & 0 & G_a & 0 & 0 & 0 & 0 \\ -2G_m & 0 & -\gamma_m & \omega_m & 0 & 0 & 0 & 0 & 0 \\ 0 & 0 & -\omega_m & -\gamma_m & 0 & 0 & 0 & 0 & 0 \\ 2G_a & 0 & 0 & 0 & M & \frac{\Omega_z}{2} & (\alpha - \frac{\delta}{2}) & 0 & 0 \\ 0 & 0 & 0 & 0 & \frac{\Omega_z}{2} & M & 0 & -(\alpha - \frac{\delta}{2}) & 0 \\ 2G_a & 0 & 0 & 0 & (-\alpha + \frac{\delta}{2}) & 0 & M & -\frac{\Omega_z}{2} & 0 \\ 0 & 0 & 0 & 0 & 0 & -(-\alpha + \frac{\delta}{2}) & -\frac{\Omega_z}{2} & M & 0 \end{pmatrix}$$

where $M = \frac{\Omega}{2} + v + UN(1 - \epsilon) - \gamma_a$, $v = g_a n_s$ and $\Omega = \hbar \mathbf{k}^2 / m_a$ is the recoil frequency of atomic states. $\alpha = \tilde{\alpha} \mathbf{k}_x$ is the effective strength of SO coupling. The evolution of the system can be analyzed by matrix \mathcal{K} , which contains multiple crucial parameters such as effective detuning $\Delta = \tilde{\Delta} - g_m q_s + g_a N$, where q_s is the steady-state quadrature of the mechanical mirror, and modified coupling of the intracavity optical mode with mechanical mirror $G_m = \sqrt{2} g_m |c_s|$ and atomic modes $G_a = \sqrt{2} g_a |c_s|$, tuned by the mean intracavity field with amplitude $c_s = \frac{\eta}{\kappa + i\Delta}$. The particular interlaced nature of these steady-state parameters provides an efficient opportunity to understand nonlinear and bistable dynamics of the system.

To make the system accurate and useful, we have to ensure stability of the system, and for this purpose we perform stability analysis of the system. The system can only be stable if the roots of the characteristic polynomial of matrix \mathcal{K} lie

in the left half of the complex plane. For this purpose, we apply the Routh-Hurwitz stability criterion [22] on matrix \mathcal{K} and numerically develop stability conditions for the system. These stability conditions are given as $M > \kappa + \gamma_m$, $(\alpha - \delta/2)^2 + M^2 > \kappa^2 + \Delta^2 - \omega_m^2 - \Omega_z^2$, $\omega_m > \Delta > \kappa > \gamma_m > 0$ and $\Delta G_a^2 + \Delta G_m^2 > M(\kappa^2 - \Omega_z^2)$. We strictly follow these conditions while performing all numerical calculations in the paper.

Furthermore, we take the Fourier transform of linearized Langevin equations to perform frequency domain analysis and solve them for position and momentum quadratures of the intracavity field

$$\delta q_c(\omega) = \frac{1}{L(\omega)} (\sqrt{2\kappa} [\Delta \delta p_c^{\text{in}} + (\kappa + i\omega) \delta q_c^{\text{in}}] + \Delta [G_a \delta q_\uparrow(\omega) + G_a \delta q_\downarrow(\omega) - G_m \delta q(\omega)]), \quad (\text{B1})$$

$$\delta p_c(\omega) = \frac{1}{L(\omega)} \left(\sqrt{2\kappa} [\Delta \delta q_c^{\text{in}} + (\kappa + i\omega) \delta p_c^{\text{in}}] + (\kappa + i\omega) \times [G_a \delta q_{\uparrow}(\omega) + G_a \delta q_{\downarrow}(\omega) - G_m \delta q(\omega)] \right), \quad (\text{B2})$$

respectively, position quadrature of atomic modes

$$\delta q_{\uparrow, \downarrow}(\omega) = \frac{1}{X(\omega)} \left((B_{\uparrow, \downarrow}(\omega) + A_{\downarrow, \uparrow}(\omega)) C(\omega) [\Delta \delta p_c^{\text{in}} + (\kappa + i\omega) \delta q_c^{\text{in}}] + L_{1,3}(\omega) f_m + L_{2,4}(\omega) f_a \right), \quad (\text{B3})$$

and finally for the position quadrature of the mechanical mirror:

$$\delta q(\omega) = \frac{1}{X_m(\omega)} \left(A_m(\omega) [\Delta \delta p_c^{\text{in}} + (\kappa + i\omega) \delta q_c^{\text{in}}] + B_m(\omega) f_m + C_m(\omega) f_a \right). \quad (\text{B4})$$

The parameter $L(\omega) = (\kappa + i\omega)^2 - \Delta^2$ contains effective detuning of the system, $W(\omega) = \gamma_a + i\omega - \Omega/2 - v - UN(1 - \varepsilon)$ and $K(\omega) = W^2(\omega) + (\alpha^2 - \delta/2)^2$ describe atom-atom interactions, and $S_m(\omega) = (\gamma_m + i\omega)^2 L(\omega) - L(\omega) \omega_m^2 + 2G_m^2 \Delta (\gamma_m + i\omega)$ is related to mirror coupling with the intracavity field. $A_{\uparrow, \downarrow}(\omega) = 4W(\omega)K(\omega)L(\omega)S_m(\omega) \pm \Omega_z^2 L(\omega)S_m(\omega) - 8G_a^2 \Delta K(\omega)S_m(\omega) + 16G_a^2 \Delta^2 G_m^2 (\gamma_m + i\omega)K(\omega)$ and $B_{\uparrow, \downarrow}(\omega) = \pm \Omega_z^2 L(\omega)S_m(\omega) + 4(\pm \alpha \mp \delta/2)K(\omega)L(\omega)S_m(\omega) + 8G_a^2 \Delta K(\omega)S_m(\omega) - 16G_a^2 \Delta^2 G_m^2 (\gamma_m + i\omega)K(\omega)$ describe the behavior of the atomic mode and its association with the moving end mirror of the system. $B_m(\omega) = 2G_m \sqrt{(2\kappa)} (\gamma_m + i\omega) X(\omega) + = 2G_m \Delta G_a [A_{\uparrow}(\omega) + A_{\downarrow}(\omega) + B_{\uparrow}(\omega) + B_{\downarrow}(\omega)]$ represents mechanical mirror behavior and its coupling with atomic modes. Further, $C(\omega) = 8G_a^2 \sqrt{(2\kappa)} K(\omega)S_m(\omega) + 16G_a^2 \sqrt{2\kappa} G_m^2 (\gamma_m + i\omega)K(\omega)$, $L_{1,3}(\omega) = [B_{\uparrow, \downarrow}(\omega) + A_{\downarrow, \uparrow}(\omega)] 8G_a^2 \sqrt{\gamma_m} \Delta K(\omega)L(\omega) (\gamma_m + i\omega)$, $L_{2,4}(\omega) = [B_{\uparrow, \downarrow}(\omega) + A_{\downarrow, \uparrow}(\omega)] 8G_a^2 \sqrt{\gamma_a} K(\omega)S_m(\omega)$, $B_m(\omega) = 2G_m \Delta G_a [L_1(\omega) + L_3(\omega)] + 2\sqrt{\gamma_m} L(\omega)X(\omega)$, and $C_m(\omega) = 2G_m \Delta G_a [L_2(\omega) + L_4(\omega)]$. The term $X(\omega) = A_{\uparrow}(\omega)A_{\downarrow}(\omega) + B_{\uparrow}(\omega)B_{\downarrow}(\omega)$ represents modified susceptibility atomic states and $X_m(\omega) = X(\omega)S_m(\omega)$ corresponds to the modified susceptibility of the mechanical mirror.

APPENDIX C: DENSITY-NOISE SPECTRUM

By using frequency domain solutions given above and standard formalism for autocorrelation, as discussed in the main text, the DNS for pseudo-spin-up and -spin-down atomic states will be read as

$$S_{\uparrow, \downarrow}(\omega, \Delta) = \frac{1}{|X(\omega)|^2} \left\{ 2\pi |C(\omega)|^2 (|B_{\uparrow, \downarrow}(\omega)|^2 + |A_{\downarrow, \uparrow}(\omega)|^2) [\Delta^2 + \kappa^2 + \omega^2] + 2\pi L_{2,4}(\omega) + L_{1,3}(\omega) \frac{\gamma_m \omega}{\omega_m} \left[1 + \coth\left(\frac{\hbar\omega}{2k_B T}\right) \right] \right\}. \quad (\text{C1})$$

Similarly, we can write the DNS equation for the mechanical mirror of the system as

$$S_m(\omega, \Delta) = \frac{1}{|X_m(\omega)|^2} \left\{ |A_m(\omega)|^2 (\Delta^2 + \kappa^2 + \omega^2) + 2\pi B_m(\omega) + C_m(\omega) \frac{\gamma_m \omega}{\omega_m} \left[1 + \coth\left(\frac{\hbar\omega}{2k_B T}\right) \right] \right\}. \quad (\text{C2})$$

APPENDIX D: SPECTRAL DENSITY OF OUTGOING OPTICAL FIELD

In order to calculate the output optical field of the system, we use the input-output field relation, $\delta q_c^{\text{out}} = \sqrt{2\kappa} \delta q_c - \delta q_c^{\text{in}}$ and $\delta p_c^{\text{out}} = \sqrt{2\kappa} \delta p_c - \delta p_c^{\text{in}}$, where $p_{\text{in}}, q_{\text{in}}$ and $p_{\text{out}}, q_{\text{out}}$ represent input and output field quadratures, respectively. By utilizing the above relation and intracavity field quadrature, we obtain the output field relation as

$$\delta q_c^{\text{out}}(\omega) = \frac{1}{L(\omega)} \left([2\kappa \Delta \delta p_c^{\text{in}} + (\kappa^2 + \omega^2 + \Delta^2) \delta q_c^{\text{in}}] + \sqrt{2\kappa} \Delta [G_a \delta q_{\uparrow}(\omega) + G_a \delta q_{\downarrow}(\omega) - G_m \delta q(\omega)] \right), \quad (\text{D1})$$

$$\delta p_c^{\text{out}}(\omega) = \frac{1}{L(\omega)} \left([2\kappa \Delta \delta q_c^{\text{in}} + (\kappa^2 + \omega^2 + \Delta^2) \delta p_c^{\text{in}}] + \sqrt{2\kappa} (\kappa + i\omega) [G_a \delta q_{\uparrow}(\omega) + G_a \delta q_{\downarrow}(\omega) - G_m \delta q(\omega)] \right). \quad (\text{D2})$$

Now, by combining position and momentum quadratures of the field, we obtain outgoing field operator c_{out} as

$$\delta c_{\text{out}}(\omega) = \frac{1}{L(\omega)} \left([2\kappa \Delta \delta c_{\text{in}}^{\dagger} + (\kappa^2 + \omega^2 + \Delta^2) \delta c_{\text{in}}] + \sqrt{2\kappa} \Delta [G_a \delta q_{\uparrow}(\omega) + G_a \delta q_{\downarrow}(\omega) - G_m \delta q(\omega)] \right). \quad (\text{D3})$$

Further, to determine the dependence of the outgoing optical mode on the external pump field power P , we redefine coupling terms as a function of P ,

$$G_m = \sqrt{2} C_S g_m = \frac{2\omega_c}{L} \sqrt{\frac{P\kappa}{m\omega_m\omega_p(\kappa^2 + \Delta^2)^2}}, \quad (\text{D4})$$

$$G_a = \sqrt{2} C_S g_a = \frac{2\omega_c}{L} \sqrt{\frac{P\kappa}{m\Omega\omega_p(\kappa^2 + \Delta^2)^2}}, \quad (\text{D5})$$

and after this we calculate the DNS of the outgoing optical mode by simply using the two frequency autocorrelation formula:

$$S_{\text{out}}(P, \omega) = \frac{2\pi}{|L(\omega)|^2} \left([\kappa^2 + \omega^2 + \Delta^2 + 2\kappa \Delta] + 4\kappa \Delta [G_a S_{\uparrow}(\omega, \Delta) + G_a S_{\downarrow}(\omega, \Delta) - G_m \delta S_m(\omega, \Delta)] \right). \quad (\text{D6})$$

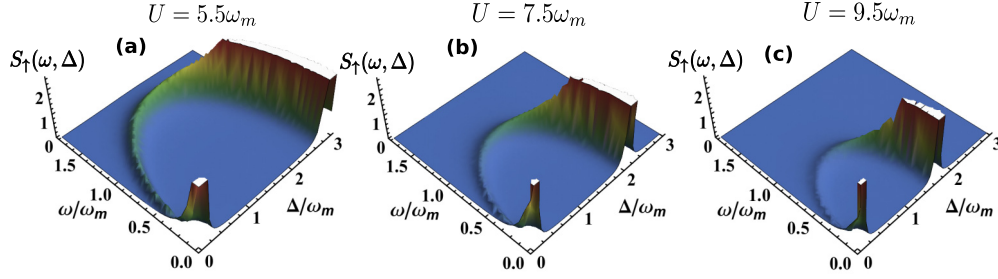


FIG. 7. The dynamics of $S_{\uparrow}(\omega, \Delta)$, as a function of detuning Δ/ω_m and frequency ω/ω_m , under the effects of many-body interactions U/ω_m . (a–c) $S_{\uparrow}(\omega, \Delta)$ with atom-atom interaction $U = 5.5\omega_m, 7.5\omega_m,$ and $9.5\omega_m$, respectively. Here, the strength of SO coupling is kept constant at $\alpha = 10\pi\omega_m$. One can observe that the strength of atom-atom interactions influences $S_{\uparrow}(\omega, \Delta)$ in a similar way as SO coupling does. By increasing U/ω_m , the area underneath $S_{\uparrow}(\omega, \Delta)$ is decreased, which leads to the cooling of the atomic mode [23]. The remaining parameters are the same as in Fig. 2.

APPENDIX E: INFLUENCE OF ATOM-ATOM INTERACTIONS ON ATOMIC DENSITY-NOISE SPECTRUM

The atom-atom interactions U/ω_m of atomic dressed states show similar influence on $S_{\uparrow}(\omega, \Delta)$ as the influence of SO coupling on the atomic dressed states, which can be seen in Figs. 7(a)–7(c), where the strength of atom-atom interactions is considered as $U = 5.5\omega_m, 7.5\omega_m, 9.5\omega_m$, respectively. The radius as well as height of the atomic DNS decrease with increase in atom-atom interactions U/ω_m of dressed states. [Note: The effects of atom-atom interactions $S_{\downarrow}(\omega, \Delta)$ are not shown here because they will be likewise as on $S_{\uparrow}(\omega, \Delta)$.] As atom-atom interactions are the combination of interspecies as well as intraspecies interactions and modify the coupling atomic states with intracavity potential, therefore, by increasing interactions, the strength of atomic backaction will be increased, leading to more self-confinement. Thus, the strength of atom-atom interactions can likely be used to control the

low-temperature dynamics of atomic dressed states as SO coupling.

APPENDIX F: MIRROR DENSITY-NOISE SPECTRUM UNDER INFLUENCE OF SO COUPLING AND ATOM-ATOM INTERACTIONS

The dynamics of the mechanical mirror will also be influenced by the existence of atomic states as atomic dressed states are influenced by the existence of the mechanical mirror. Figure 8 demonstrates $S_m(\omega, \Delta)$ as a function of Δ/ω_m and ω/ω_m , under the influence of SO coupling and atom-atom interaction. The atom-field coupling is considered as $G_a = 4.1\omega_m$ while the mirror-field coupling is taken as $G_m = 1.5\omega_m$. The behavior of $S_m(\omega, \Delta)$ in the absence of SO coupling is shown in Fig. 8(a), which is similar to the behavior of the atomic DNS. A semicircular structure appears with increase in detuning Δ/ω_m towards frequency ω/ω_m . The

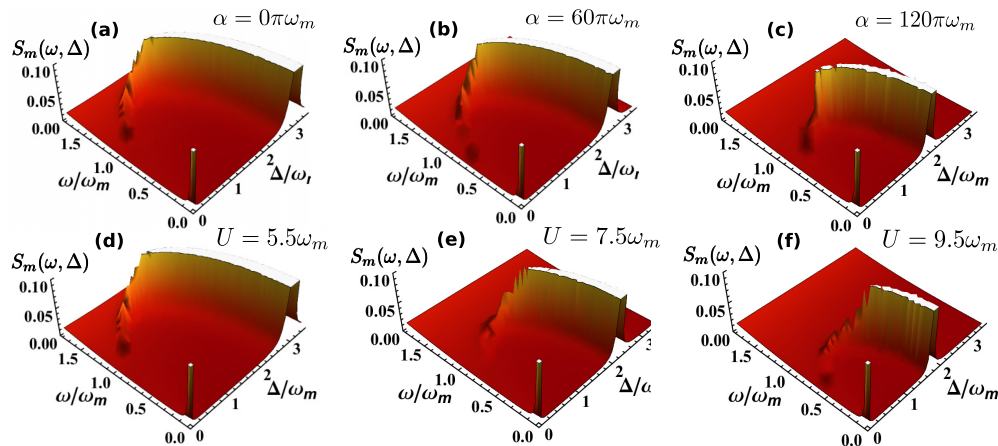


FIG. 8. Density-noise spectrum (DNS) $S_m(\omega, \Delta)$ (in units of W/Hz) for a mechanical mirror of the system vs normalized effective detuning Δ/ω_m and frequency ω/ω_m under the influence of spin-orbit (SO) coupling α/ω_m of atomic spin states and normalized atom-atom interactions U/ω_m among atomic states. (a) $S_m(\omega, \Delta)$ in the absence of SO coupling $\alpha = 0\pi\omega_m$ with atom-atom interactions $U = 5.5\omega_m$. The color configuration corresponds to the strength of mechanical mirror DNS [$S_m(\omega, \Delta)$]. (b,c) Behavior of $S_m(\omega, \Delta)$ under the influence of $\alpha = 60\pi\omega_m$ and $120\pi\omega_m$, respectively. The dynamics of $S_m(\omega, \Delta)$ under the effects of many-body interactions U/ω_m are illustrated in (d–f). (d–f) $S_m(\omega, \Delta)$ as a function of Δ/ω_m and ω/ω_m with atom-atom interaction $U = 5.5\omega_m, 7.5\omega_m,$ and $9.5\omega_m$, respectively, while the strength of SO coupling is kept constant at $\alpha = 10\pi\omega_m$. The atom-field coupling is considered as $G_a = 4.1\omega_m$ while the mirror-field coupling is taken as $G_m = 1.5\omega_m$. The remaining parameters, used in numerical calculations, are the same as in Fig. 2.

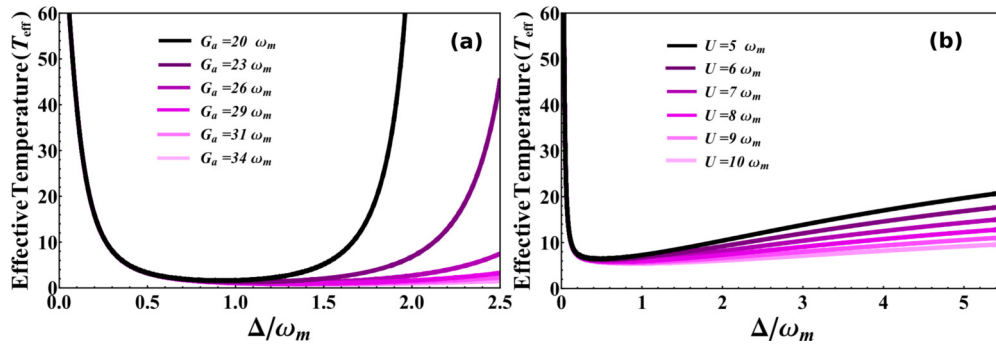


FIG. 9. (a) Effective temperature T_{eff} of a mechanical mirror under the influence of G_a/ω_m . The SO coupling strength is now considered as $\alpha = 100\pi\omega_m$ and many-body interaction is kept as $U = 5.5\omega_m$. The black curve represents $G_a = 20\omega_m$ while magenta curves from dark shade to light shade are for atom-field coupling $G_a = 23\omega_m, 26\omega_m, 29\omega_m, 31\omega_m$, and $34\omega_m$, respectively. Similarly, (c) deals with the behavior effective temperature T_{eff} of a mechanical mirror under the influence of U/ω_m at $\alpha = 100\pi\omega_m$ and $G_a = 20\omega_m$. Similarly, the black curve represents $U = 5\omega_m$ while magenta curves from dark shade to light shade represent atom-atom interactions $U = 6\omega_m, 7\omega_m, 8\omega_m, 9\omega_m$, and $10\omega_m$, respectively. The other parameters used in numerical calculation are the same as in Fig. 2.

height of $S_m(\omega, \Delta)$ decreases initially and achieves the optimal cooling point. However, when the system detuning is further increased from $\Delta = 1\omega_m$, the $S_m(\omega, \Delta)$ shows rapid increase in the height of the structure giving rise to the temperature of the mechanical mirror.

The strength of SO coupling induces similar influence as it does on the atomic DNS. The radius of the structure is suppressed by the increased SO coupling, as shown in Figs. 8(b) and 8(c), where the strength of SO coupling is increased to $\alpha = 60\omega_m$ and $130\omega_m$, respectively. Not only SO coupling but also the atom-atom interactions of atomic dressed states will show similar effects on the mechanical DNS as they are inducing in the atomic DNS. The increase in atom-atom interactions will also reduce the radius of the semicircular structure, as shown in Figs. 8(d)–8(f), where the strength of atom-atom interactions is increased to $U = 5.5\omega_m, 7.7\omega_m$, and $9.5\omega_m$, respectively. The SO coupling and atom-atom interactions modify the atomic density mode excitation leading to the variation in the intracavity optical spectrum in the form of modified atomic backaction which will consequently lead to the absorption of more mirror excitations by spin states. It can also be considered as the atomic and mechanical states are connected with each other through intracavity radiation

pressure, acting as a spring between these two independent entities; therefore, the modifications produced by SO coupling and atom-atom interaction will show similar influence on the mechanical mirror as they are producing on atomic dressed states [23].

APPENDIX G: INFLUENCE OF ATOM-FIELD COUPLING AND ATOM-ATOM INTERACTIONS ON MECHANICAL MIRROR TEMPERATURE

If we increase the atomic mode coupling with intracavity field, atomic dressed states will absorb more phonons emitted by the mechanical mirror of the system which will decrease the thermal excitation of mechanical mirror. Figure 9(a) shows such influence of atom-field coupling on the mechanical oscillator of the system where the effective temperature of the mirror is decreased by increasing atom-field coupling [21]. The atom-atom interactions of the atomic mode will also influence the mechanical mirror similarly as SO coupling has shown [23]. The atom-atom interactions also contribute to control the thermal excitation of the mechanical mirror, which leads to cool the oscillating mirror to its quantum-mechanical ground state, as shown in Fig. 9(b).

- [1] T. J. Kippenberg and K. J. Vahala, *Science* **321**, 1172 (2008); M. Aspelmeyer, T. J. Kippenberg, and F. Marquardt, *Rev. Mod. Phys.* **86**, 1391 (2014).
- [2] T. J. Kippenberg and K. J. Vahala, *Opt. Express* **17**, 20911 (2009).
- [3] P. Meystre, *Ann. Phys.* **525**, 215 (2013).
- [4] A. D. O’Connell *et al.*, *Nature (London)* **464**, 697 (2010).
- [5] J. D. Teufel *et al.*, *Nature (London)* **475**, 359 (2011).
- [6] J. Chan *et al.*, *Nature (London)* **478**, 89 (2011).
- [7] M. Yuan *et al.*, *Nat. Commun.* **6**, 8491 (2015).
- [8] O. Arcizet *et al.*, *Nature (London)* **444**, 71 (2006).
- [9] S. Gigan *et al.*, *Nature (London)* **444**, 67 (2006).
- [10] D. Kleckner and D. Bouwmeester, *Nature (London)* **444**, 75 (2006).
- [11] A. Schliesser, P. Del’Haye, N. Nooshi, K. J. Vahala, and T. J. Kippenberg, *Phys. Rev. Lett.* **97**, 243905 (2006).
- [12] J. D. Teufel, J. W. Harlow, C. A. Regal, and K. W. Lehnert, *Phys. Rev. Lett.* **101**, 197203 (2008).
- [13] D. J. Wilson *et al.*, *Nature (London)* **524**, 325 (2015).
- [14] I. Wilson-Rae, N. Nooshi, W. Zwerger, and T. J. Kippenberg, *Phys. Rev. Lett.* **99**, 093901 (2007).
- [15] E. E. Wollman *et al.*, *Science* **349**, 952 (2015).
- [16] A. Nigués, A. Siria, and P. Verlot, *Nat. Commun.* **6**, 8104 (2015).
- [17] K. W. Murch *et al.*, *Nature Physics* **4**, 561 (2008).
- [18] F. Brennecke *et al.*, *Science* **322**, 235 (2008).
- [19] K. A. Yasir and W. M. Liu, *Sci. Rep.* **5**, 10612 (2015).
- [20] K. A. Yasir and W. M. Liu, *Sci. Rep.* **6**, 22651 (2016).
- [21] M. Paternostro *et al.*, *New J. Phys.* **8**, 107 (2006).

- [22] M. Paternostro, G. De Chiara, and G. M. Palma, *Phys. Rev. Lett.* **104**, 243602 (2010).
- [23] S. Mahajan, N. Aggarwal, A. B. Bhattacharjee, and ManMohan, *J. Phys. B* **46**, 085301 (2013).
- [24] Y. C. Liu, Y. F. Xiao, X. Luan, and C. W. Wong, *Phys. Rev. Lett.* **110**, 153606 (2013).
- [25] F. Elste, S. M. Girvin, and A. A. Clerk, *Phys. Rev. Lett.* **102**, 207209 (2009).
- [26] D. W. C. Brooks *et al.*, *Nature (London)* **488**, 476 (2012).
- [27] K. Zhang, F. Bariani, and P. Meystre, *Phys. Rev. Lett.* **112**, 150602 (2014).
- [28] A. H. Safavi-Naeini *et al.*, *New J. Phys.* **15**, 035007 (2013).
- [29] Y. Yanay, J. C. Sankey, and A. A. Clerk, *Phys. Rev. A* **93**, 063809 (2016).
- [30] P. Weber *et al.*, *Nat. Commun.* **7**, 12496 (2016).
- [31] V. Galitski and I. B. Spielman, *Nature (London)* **494**, 49 (2013).
- [32] X. J. Liu, M. F. Borunda, X. Liu, and J. Sinova, *Phys. Rev. Lett.* **102**, 046402 (2009).
- [33] Y. J. Lin *et al.*, *Nature (London)* **462**, 628 (2009).
- [34] Y. K. Kato *et al.*, *Science* **306**, 1910 (2004).
- [35] M. König *et al.*, *Science* **318**, 766 (2007).
- [36] B. A. Bernevig, T. L. Hughes, and S. C. Zhang, *Science* **314**, 1757 (2006).
- [37] D. Hsieh *et al.*, *Nature (London)* **452**, 970 (2008).
- [38] C. Hamner *et al.*, *Nat. Commun.* **5**, 4023 (2014).
- [39] K. Sun *et al.*, *Nat. Phys.* **8**, 67 (2012).
- [40] J. D. Koralek *et al.*, *Nature (London)* **458**, 610 (2009).
- [41] C. Hamner, Y. Zhang, M. A. Khamehchi, M. J. Davis, and P. Engels, *Phys. Rev. Lett.* **114**, 070401 (2015).
- [42] Y. J. Lin, K. Jiménez-García, and I. B. Spielman, *Nature (London)* **471**, 83 (2011).
- [43] H. Hu, B. Ramachandhran, H. Pu, and X. J. Liu, *Phys. Rev. Lett.* **108**, 010402 (2012).
- [44] L. Jiang, E. Tiesinga, X.-J. Liu, H. Hu, and H. Pu, *Phys. Rev. A* **90**, 053606 (2014).
- [45] X. F. Zhou, Z. W. Zhou, C. Wu, and G. C. Guo, *Phys. Rev. A* **91**, 033603 (2015).
- [46] Z. Cai, X. Zhou, and C. Wu, *Phys. Rev. A* **85**, 061605(R) (2012).
- [47] S. W. Su, I. K. Liu, Y. C. Tsai, W. M. Liu, and S. C. Gou, *Phys. Rev. A* **86**, 023601 (2012); S. W. Su *et al.*, *ibid.* **84**, 023601 (2011).
- [48] Y. Yi-Xiang, J. Ye, and W. M. Liu, *Phys. Rev. A* **90**, 053603 (2014); S. S. Zhang *et al.*, *ibid.* **87**, 063623 (2013).
- [49] N. Goldman *et al.*, *Rep. Prog. Phys.* **77**, 126401 (2014).
- [50] J. Dalibard *et al.*, *Rev. Mod. Phys.* **83**, 1523 (2011).
- [51] X. Zhou, Y. Li, Z. Cai, and C. Wu, *J. Phys. B* **48**, 249501 (2015).
- [52] C. Wu, M. S. Ian, and X. F. Zhou, *Chin. Phys. Lett.* **28**, 097102 (2011).
- [53] Y. Deng, J. Cheng, H. Jing, and S. Yi, *Phys. Rev. Lett.* **112**, 143007 (2014).
- [54] B. Padhi and S. Ghosh, *Phys. Rev. A* **90**, 023627 (2014).
- [55] L. Dong, L. Zhou, B. Wu, B. Ramachandhran, and H. Pu, *Phys. Rev. A* **89**, 011602(R) (2014).
- [56] L. Dong, C. Zhu, and H. Pu, *Atoms* **3**, 182 (2015).
- [57] J. S. Bennett *et al.*, *New J. Phys.* **18**, 053030 (2016).
- [58] I. Wilson-Rae *et al.*, *New J. Phys.* **10**, 095007 (2008).
- [59] M. Punk, D. Chowdhury, and S. Sachdev, *Nat. Phys.* **10**, 289 (2014).
- [60] H. Miyake, G. A. Siviloglou, G. Puentes, D. E. Pritchard, W. Ketterle, and D. M. Weld, *Phys. Rev. Lett.* **107**, 175302 (2011).
- [61] S. Sachdev, *Science* **288**, 475 (2000).
- [62] R. Landig *et al.*, *Nat. Commun.* **6**, 7046 (2015).
- [63] A. L. Fetter, *Phys. Rev. A* **89**, 023629 (2014).
- [64] C. Maschler, I. B. Mekhov, and H. Ritsch, *Eur. Phys. J. D* **46**, 545 (2008).
- [65] J. Higbie and D. M. Stamper-Kurn, *Phys. Rev. A* **69**, 053605 (2004).
- [66] S. Fölling *et al.*, *Nature (London)* **434**, 481 (2005).
- [67] J. M. Pirkkalainen *et al.*, *Nat. Commun.* **6**, 6981 (2015).
- [68] G. Birkl, M. Gatzke, I. H. Deutsch, S. L. Rolston, and W. D. Phillips, *Phys. Rev. Lett.* **75**, 2823 (1995).